

**Online Resource 1:** A collection of supplementary figures.

**Title:** Mixing and Finger Morphologies in Miscible Non-Newtonian Fluid Displacement

**Authors:** Nicole Mehr ([mehrn@oregonstate.edu](mailto:mehrn@oregonstate.edu)<sup>1</sup>), Clément Roques

([clement.roques@erdw.ethz.ch](mailto:clement.roques@erdw.ethz.ch))<sup>2</sup>, Yves Méheust ([yves.meheust@univ-rennes1.fr](mailto:yves.meheust@univ-rennes1.fr))<sup>3</sup>, Skip

Rocheffort ([skip.rocheffort@oregonstate.edu](mailto:skip.rocheffort@oregonstate.edu))<sup>1</sup>, John S. Selker

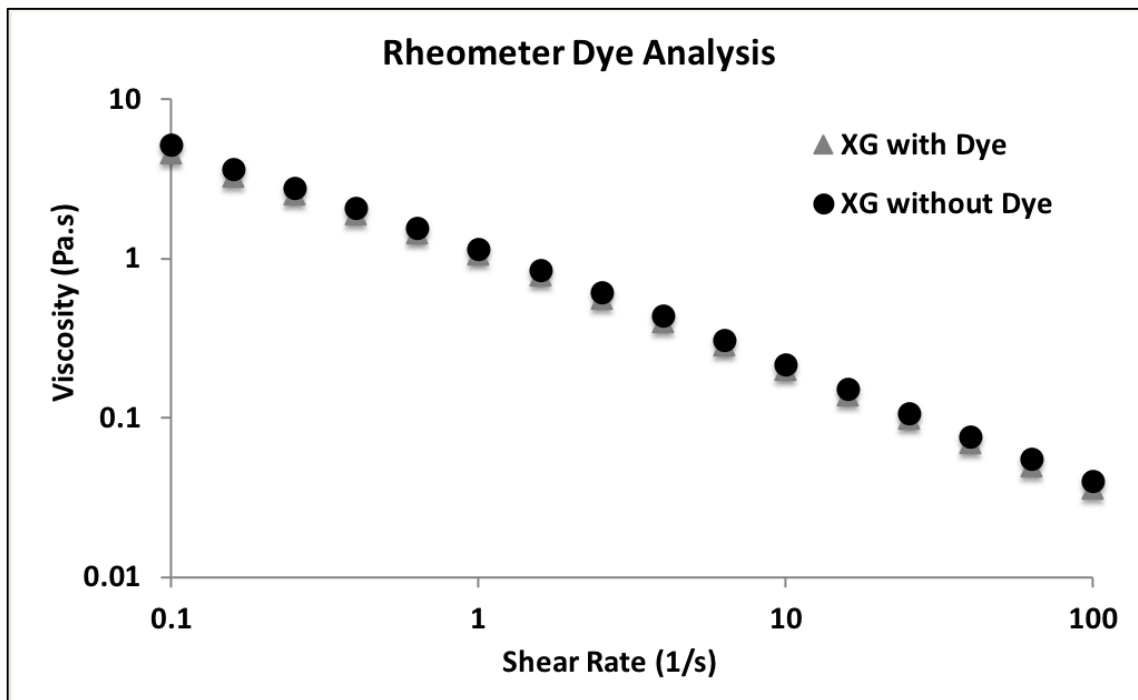
([John.Selker@oregonstate.edu](mailto:John.Selker@oregonstate.edu))<sup>1</sup>

**Affiliations:** <sup>1</sup>Oregon State University, Biological and Ecological Engineering Department, OR, USA.

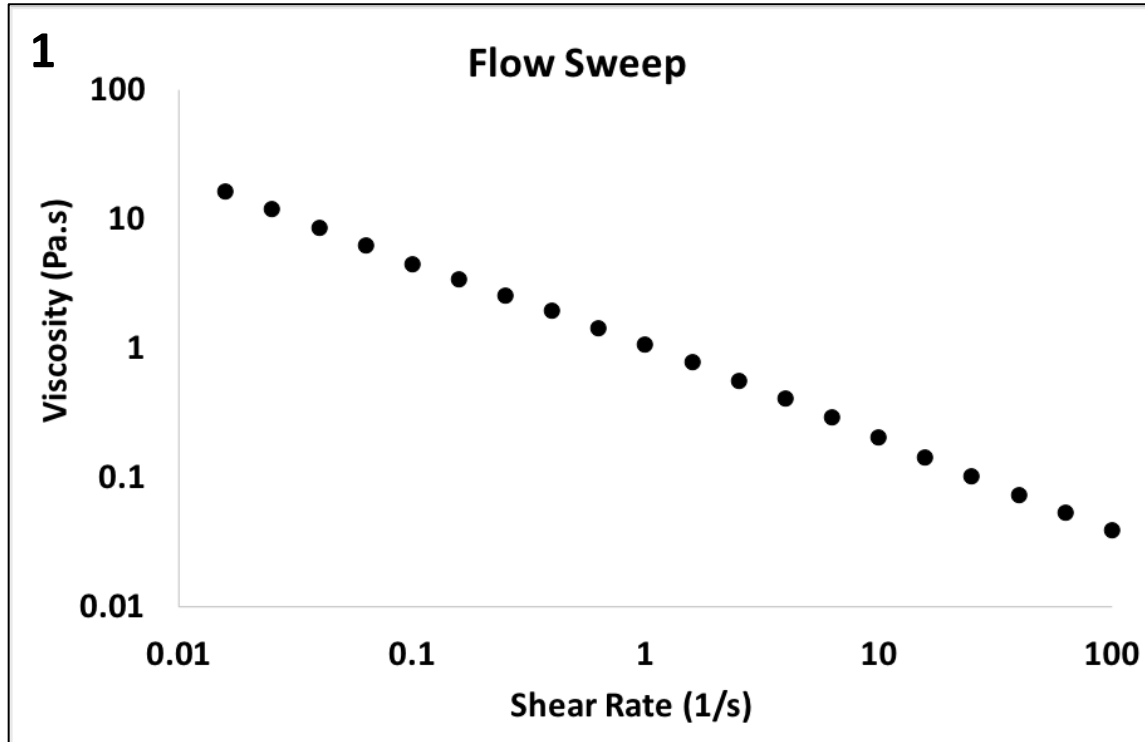
<sup>2</sup>ETH Zürich, Department of Earth Sciences, Sonneggstrasse 5, Zürich, Switzerland.

<sup>3</sup>University Rennes, CNRS, Géosciences Rennes, UMR 6118, 35000 Rennes, France

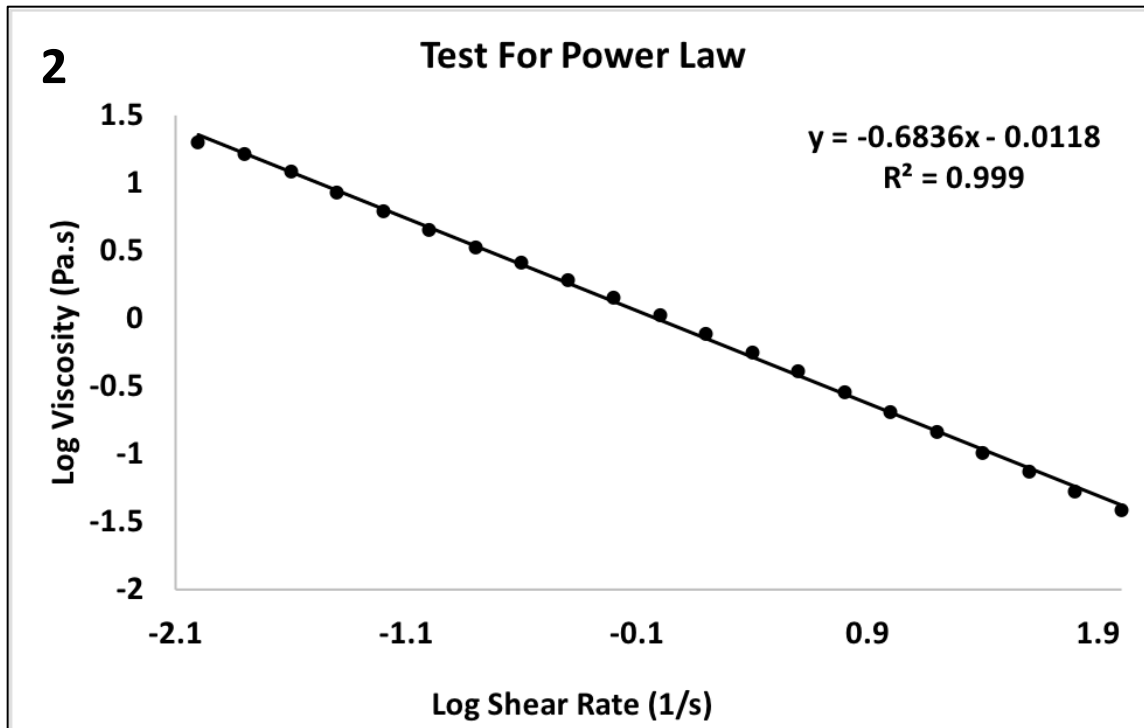
**Corresponding Author:** John Selker, [John.Selker@oregonstate.edu](mailto:John.Selker@oregonstate.edu) 541-737-6304



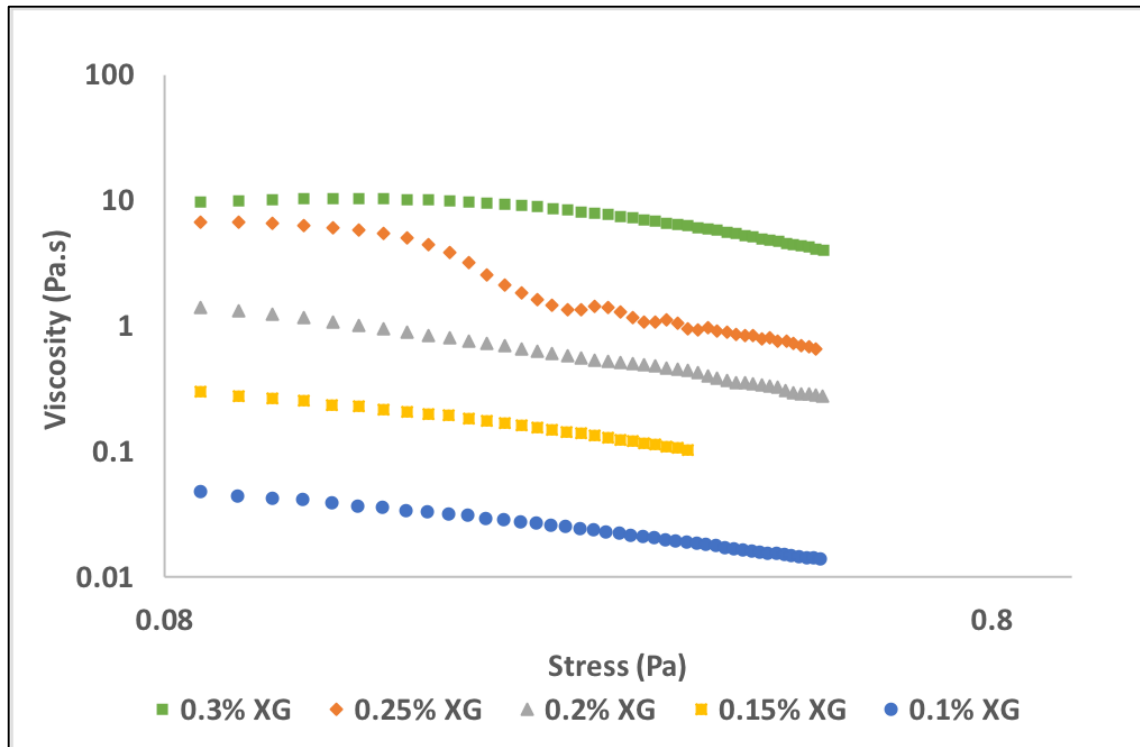
**Online Resource 1.A:** Flow sweep using a stainless-steel, cone and plate geometry on a DHR-3 rheometer to determine the effect, if any, the dye would have on the rheology of the solution. Results were plotted for a XG solution with and without added dye. The addition of powdered dye to the XG solution did not impact the solution's rheology at the low concentration of 0.025 wt.% as the curves are practically the same



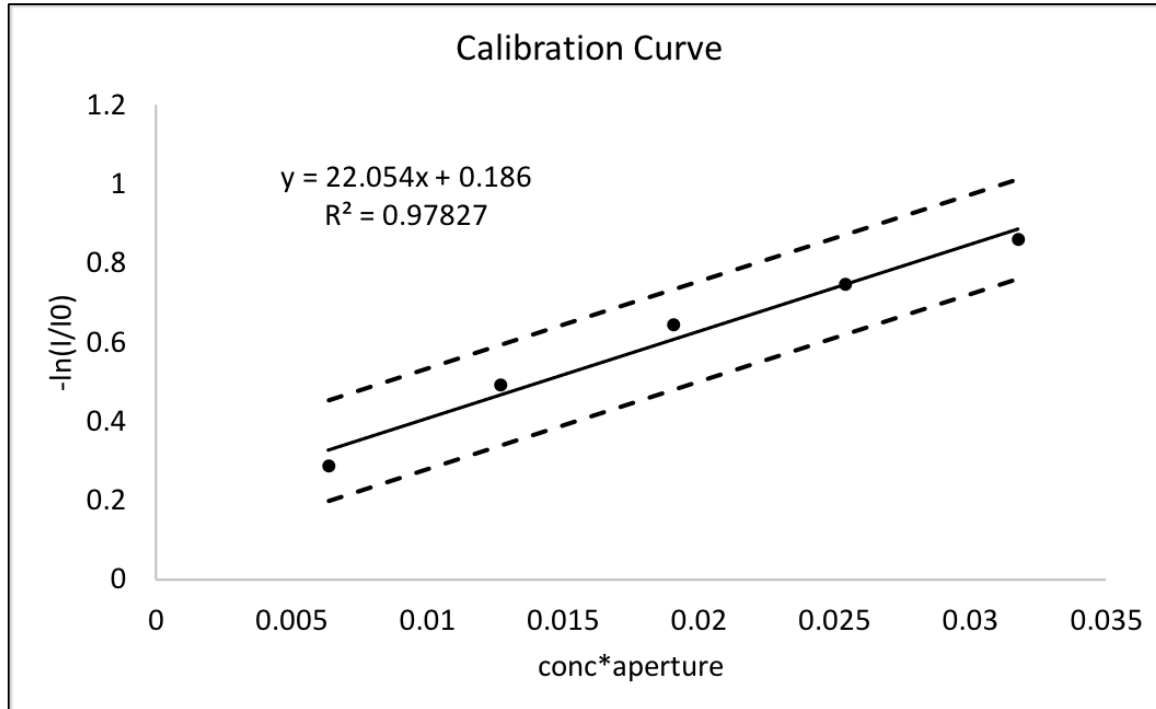
**Online Resource 1.B** An example flow sweep using a stainless-steel, cone and plate geometry on a DHR-3 rheometer, which was performed prior to each experimental run to ensure the reproducibility of the XG solutions' rheology



**Online Resource 1.C** A power law function was found to be consistent with the viscosity and shear rate curves with a power law index of  $n=0.3$  ( $0 < n < 1$ ). 0.3 was obtained from  $n-1=-0.7$  from the slope of the fitted line



**Online Resource 1.D** Plot of viscosity and stress curves obtained from using a stainless-steel, cone and plate geometry on a DHR-3 rheometer for various concentrations of XG (0.1%-0.3% concentration XG). No yield stress was observed at the concentration of 0.3% XG, which was the concentration used for the study

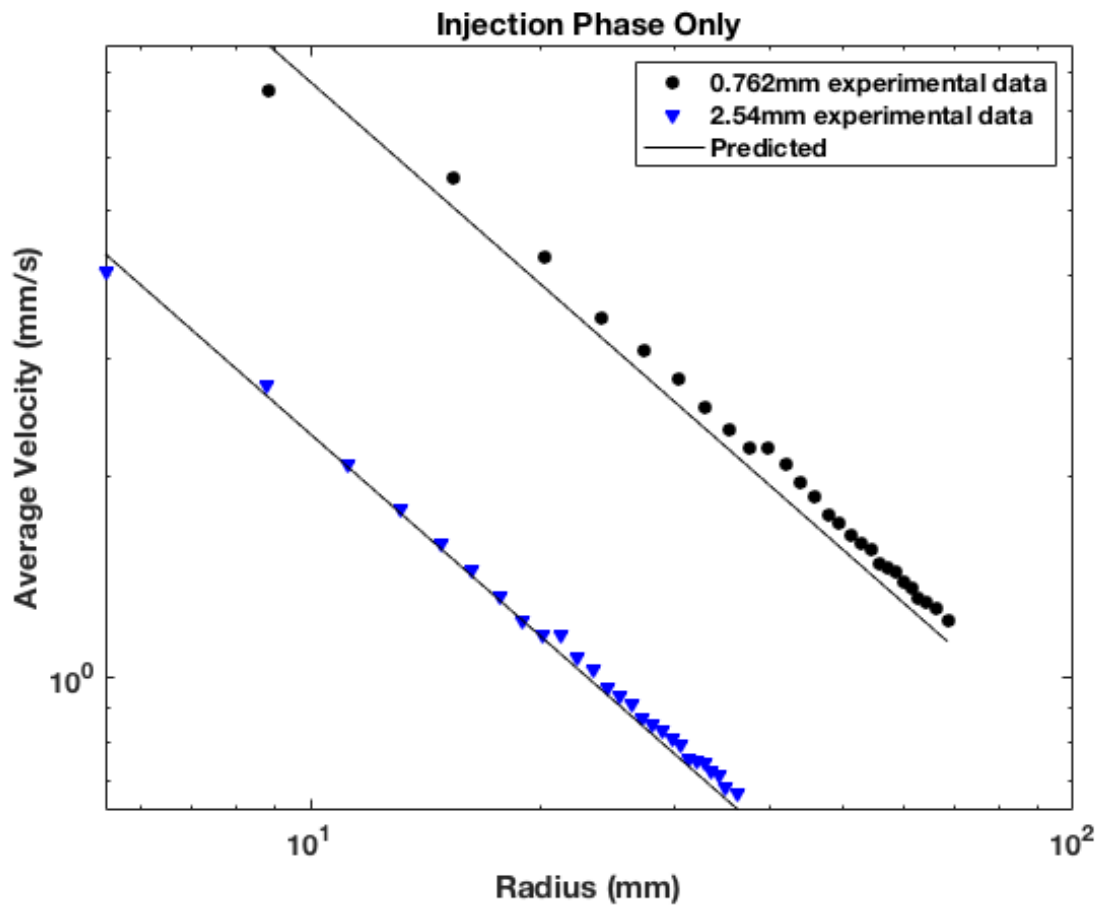


**Online Resource 1.E** Calibration curve which relates pixel intensity to concentration of XG. The calibration curve was constructed using the Beer-Lambert Law, which is written below. The upper and lower confidence intervals are denoted by the dashed lines. The natural log of pixel intensity over background light intensity and concentration\*aperture follows a linear relationship. The lower 95% confidence interval was used for image analysis

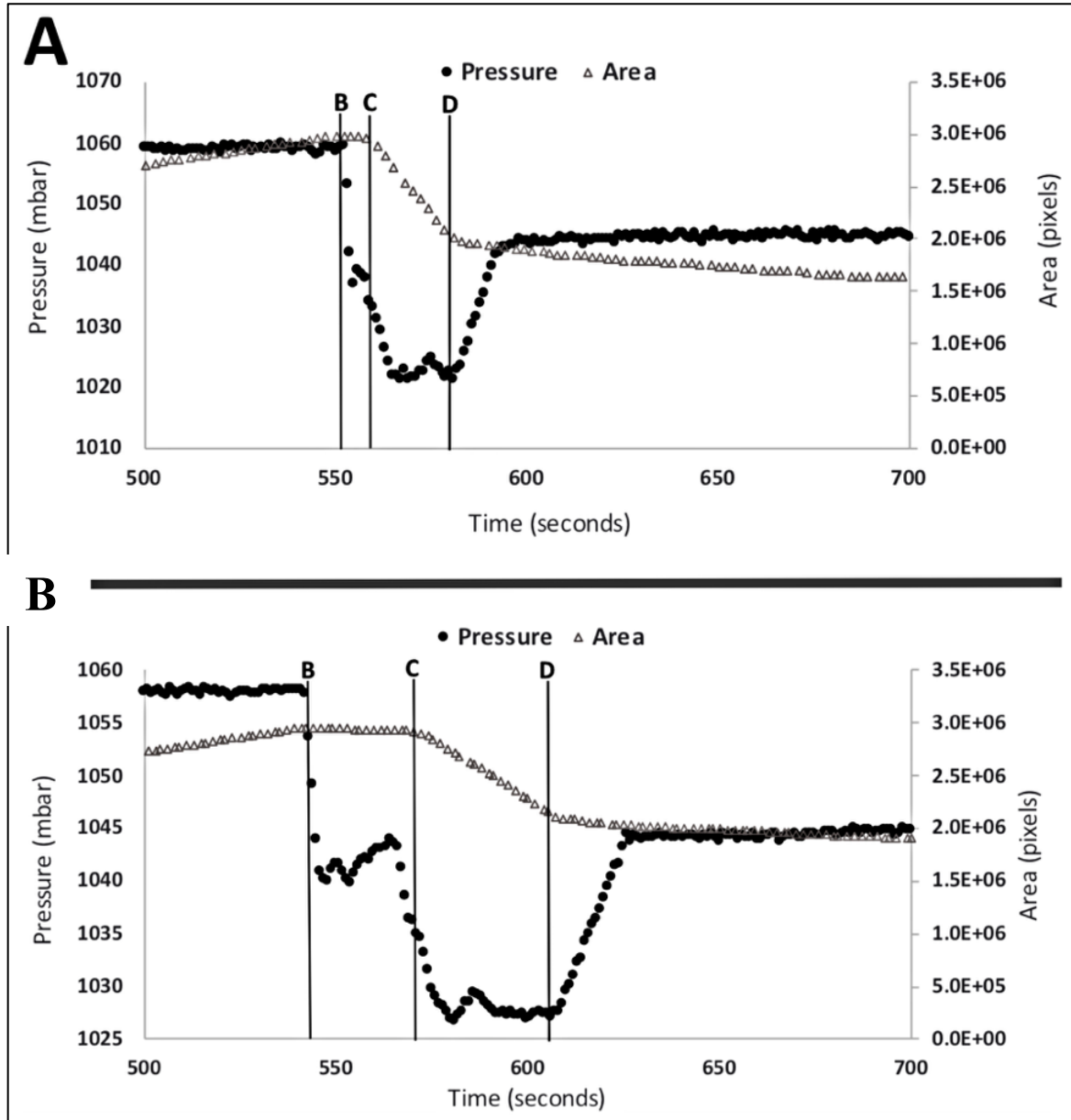
$$I = I_0 e^{za}$$

$$\ln \frac{I}{I_0} = abc$$

$a$  is the aperture,  $z$  is the absorbance,  $I$  is the intensity  $I_0$  is the background intensity,  $c$  is concentration and  $b$  is a constant.

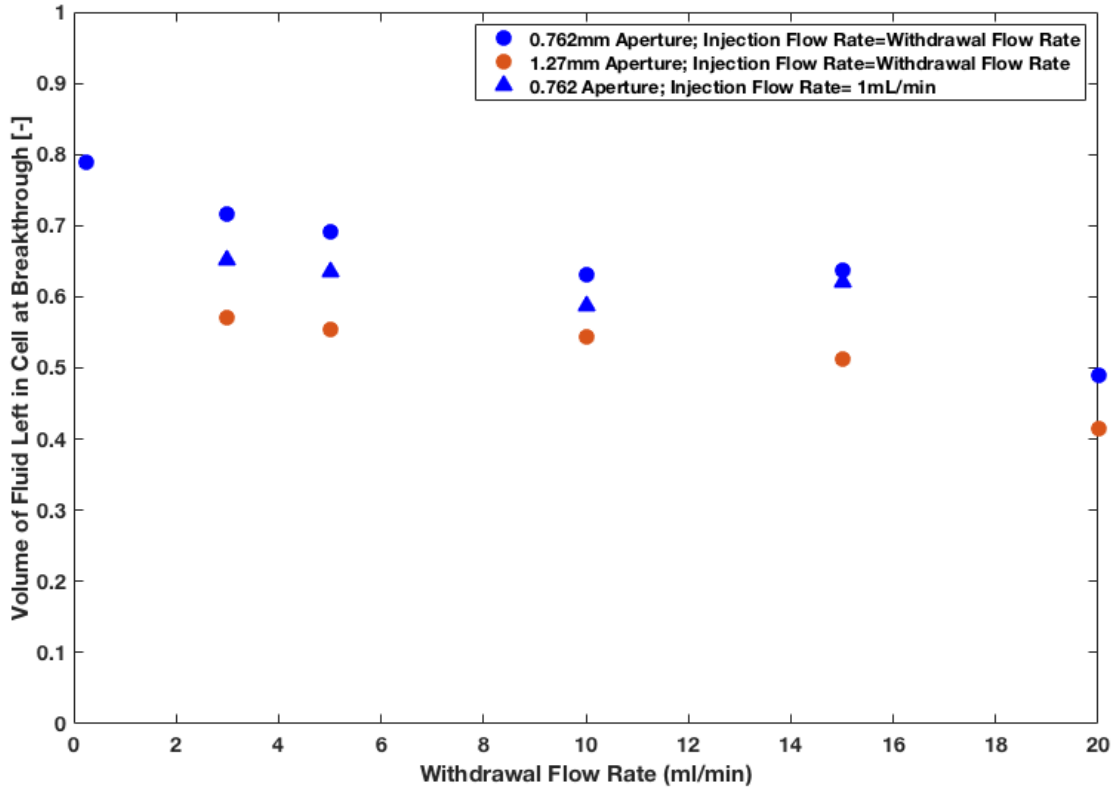


**Online Resource 1.F** Average interface velocity is plotted against mean radial distance of the interface for the injection phase. The mean velocity of the interface follows a  $\frac{1}{r}$  relationship. A power law function with a, *b* exponent of -1 is fit to the data

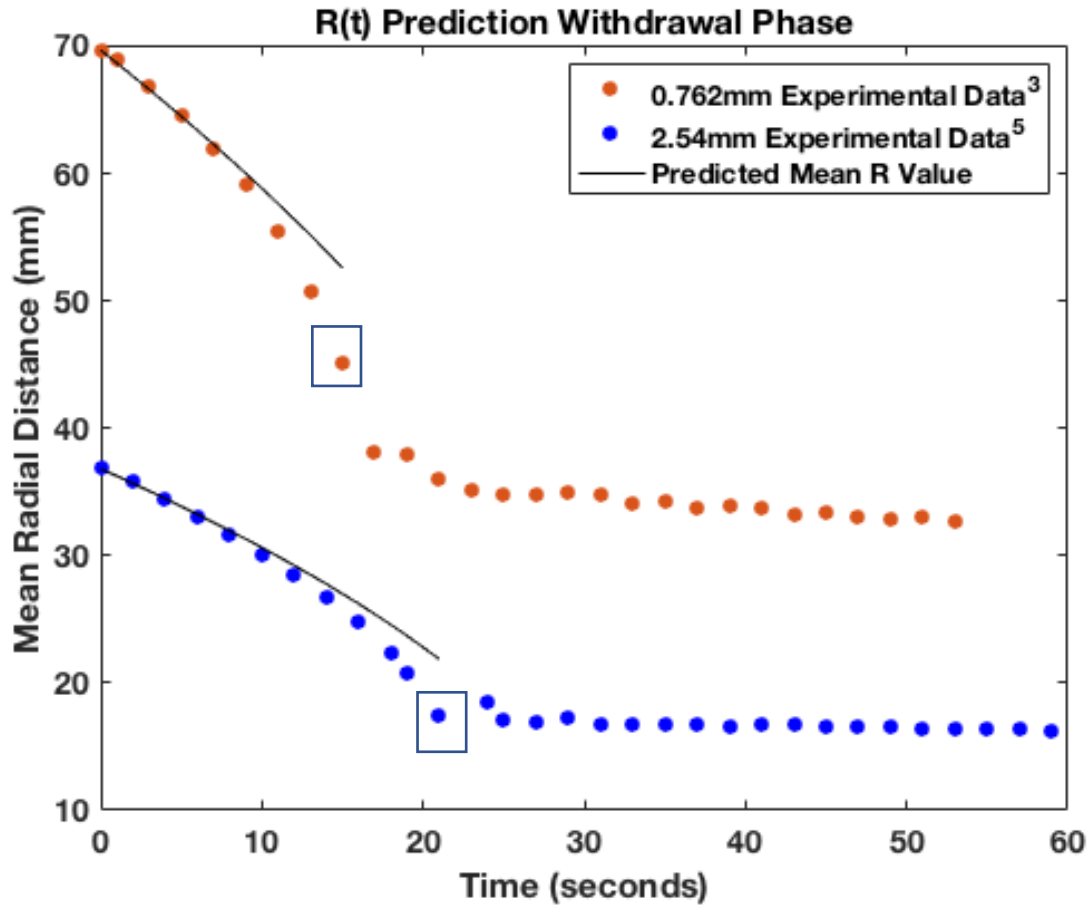


**Online Resource 1.G** Pressure data measured by the inline pressure sensor and the regional area of injected XG obtained by image analysis is plotted. **(A)** Data from an experiment with an injection rate of 1 ml/min and a withdrawal rate of 10 ml/min. **(B)** Data from an experiment with an injection rate of 1 ml/min and a withdrawal rate of 5 ml/min. Area of the XG region increased during the injection phase and decreased during the withdrawal phase. A pressure signal and area signal were detected as the XG dynamically moved in the Hele-Shaw cell. Changes in pressure and area data can be seen clearly as the syringe pump switched from the injection phase to the withdrawal phase. The first line, B, marks the end of the injection phase. The second line, C, marks the start of the withdrawal phase. The third line, D, marks the time when the first

instability reached the withdrawal site. The pressure and area data confirm that the lag time between letters B and C was due to hysteresis in the syringe pump



**Online Resource 1.H** Volume of XG in the cell at breakthrough of the first finger is plotted against flow rate. Experiments with two sets of apertures are plotted with various flow rates. A mixing fringe was observed in the 0.762mm aperture experiments (blue circles) while a mixing fringe was not observed in the 1.27mm aperture experiments (orange circles). For both sets of apertures, as flow rate increased, the volume of fluid left in the cell at finger breakthrough decreased. The higher the flow rate, the lower the viscosity ratio for the XG and water. Therefore, instability development is delayed longer for the higher flow rates. Thus, allowing a higher volume of XG to exit the cell. The blue triangles represent data from experiments with a slow injection rate of 1 mL/min and fast withdrawal rate. The slow injection rate was used to prevent the formation of the mixing fringe. More fluid was recovered when the mixing fringe was not present



**Online Resource 1.I** The mean radial distance for all points along the perimeter of the interface is plotted against time for the withdrawal phase. Two experiments are shown, both with a 20 mL/min flow rate and with either a 0.762mm or 2.54mm aperture. The experimental data fit the prediction for early times when the interface began to advance toward the injection site while still preserving a radial interface. Once apparent instabilities started forming as expected, the mean radial distance could not be predicted. The breakthrough of the first finger to the injection site is identified by the two black square boxes. After breakthrough, the system reached a quasi-steady state as mainly water exited the Hele-Shaw cell through the water channels